AFRL-AFOSR-JP-TR-2018-0038

Radar Control | Optimal Resource Allocation

Bill Moran
ROYAL MELBOURNE INSTITUTE OF TECHNOLOGY

04/17/2018
Final Report

Air Force Research Laboratory
AF Office Of Scientific Research (AFOSR)/ IOA
Arlington, Virginia 22203
Air Force Materiel Command

REPORT DOCUMENTATION PAGE

Form Approved
OMB No. 0704-0188

1. REPORT DATE *(DD-MM-YYYY)*	2. REPORT TYPE	3. DATES COVERED *(From - To)*
14-05-2018	Final	23 Sep 2015 to 22 Sep 2017

4. TITLE AND SUBTITLE
Radar Control | Optimal Resource Allocation

5a. CONTRACT NUMBER

5b. GRANT NUMBER
FA2386-15-1-4066

5c. PROGRAM ELEMENT NUMBER
61102F

6. AUTHOR(S)
Bill Moran

5d. PROJECT NUMBER

5e. TASK NUMBER

5f. WORK UNIT NUMBER

7. PERFORMING ORGANIZATION NAME(S) AND ADDRESS(ES)
ROYAL MELBOURNE INSTITUTE OF TECHNOLOGY
124 LATROBE ST
MELBOURNE, 3000 AU

8. PERFORMING ORGANIZATION REPORT NUMBER

9. SPONSORING/MONITORING AGENCY NAME(S) AND ADDRESS(ES)
AOARD
UNIT 45002
APO AP 96338-5002

10. SPONSOR/MONITOR'S ACRONYM(S)
AFRL/AFOSR IOA

11. SPONSOR/MONITOR'S REPORT NUMBER(S)
AFRL-AFOSR-JP-TR-2018-0038

12. DISTRIBUTION/AVAILABILITY STATEMENT
A DISTRIBUTION UNLIMITED: PB Public Release

13. SUPPLEMENTARY NOTES

14. ABSTRACT
This project investigated several problems in radar waveforms, waveform scheduling, and their implementation. Scheduling of sequences of radar waveforms, as in cognitive radar, has been shown, at least in simulations, to provide significantly improved performance over conventional rigid transmission of waveforms. The research and development were carried out in three research fronts: 1) Radar waveform scheduling, in particular, the development of feasible statistical signal processing techniques for sidelobe suppression and improved radar detection under Golay complementary waveforms. 2) Sensor trajectory optimisation in optimal sensor control. The development is demonstrated in the application of tracking a moving target using two passive mobile sensors. 3) Game theoretic formation of target tracking. This concept is demonstrated in an example of optimizing trajectories of two moving platforms with similar capabilities of motion and sensing. SF298It was shown that the Expected Renyi Divergence function approximated through linearization has a significantly weak correlation between the two sensor states, and thus, the trajectory scheduling performance using it is as poor as using the Trace of FIM. On the other hand, the Determinant of FIM is an appropriate statistical reward function to be used. This conclusion is confirmed by the simulation results presented. Although this work is based on tracking a moving target by two bearing-only sensors scenario, the results can also be applied to other types of sensors which are required to be used jointly to observe the underlying target state, such as Doppler radars.

15. SUBJECT TERMS
Radar, Cognitive, doppler, waveforms

16. SECURITY CLASSIFICATION OF:			17. LIMITATION OF ABSTRACT	18. NUMBER OF PAGES	19a. NAME OF RESPONSIBLE PERSON
a. REPORT	b. ABSTRACT	c. THIS PAGE			WINDER, SHEENA
Unclassified	Unclassified	Unclassified	SAR	29	19b. TELEPHONE NUMBER *(Include area code)* +81-42-511-2008

Standard Form 298 (Rev. 8/98)
Prescribed by ANSI Std. Z39.18

AOARD Project Final Report under Grant No. FA2386-15-1-4066

Project Title:

Radar Control - Optimal Resource Allocation

March 2018

Principal Investigators (PI and Co-PIs):

Prof Bill Moran (*bill.moran@rmit.edu.au/wmoran@unimelb.edu.au*)

Dr Sofia Suvorova (*sofia.suvorova@unimelb.edu.au*)

Dr Xuezhi Wang (*xuezhi.wang@rmit.edu.au*)

Prof Luiping Wang (*liuping.wang@rmit.edu.au*)

Contributors:

Dr Branko Ristic (*branko.ristic@rmit.edu.au*)

Prof Tim Brown (*tim.brown@unimelb.edu.au*)

Dr Simon Williams (*simon.williams@rmit.edu.au*)

PhD Students: Mr Yanbo Yang, Mr Keith Ing, Mr Jiahua Zhu

Period of Performance: 23 September 2015 – 22 September 2017

Institution: Signal Processing and Sensor Control Group, School of Engineering, Royal Melbourne Institute of Technology University

Mailing Address: 376 Swanston Street, Melbourne, Victoria, Australia 3000

Phone: + 61 3 9925 8098 **Fax:**

Contents

Abstract

This project investigates several problems in radar waveforms, waveform scheduling, and their implementation and it is funded by the Asian Office of Aerospace Research & Development (AOARD)/AFRL during two year period. Scheduling of sequences of radar waveforms, as in cognitive radar, has been shown, at least in simulations, to provide significantly improved performance over conventional rigid transmission of waveforms. The research and development were carried out in three research fronts:

- Radar waveform scheduling, in particular, the development of feasible statistical signal processing techniques for sidelobe suppression and improved radar detection under Golay complementary waveforms.
- Sensor trajectory optimisation in optimal sensor control. The development is demonstrated in the application of tracking a moving target using two passive mobile sensors.
- Game theoretic formation of target tracking. This concept is demonstrated in an example of optimizing trajectories of two moving platforms with similar capabilities of motion and sensing.

The research in this project has yielded 5 refereed journal papers and 4 international refereed conference papers. In addition, two journal papers are in preparation.

1 Introduction

This project investigates several problems in radar waveforms, waveform scheduling, and their implementation and it is funded by the Asian Office of Aerospace Research & Development (AOARD)/AFRL during two year period.

1.1 Summary

The problem areas here are vast and there are many avenues to pursue, including, specifically, issues around computational and other hardware resources. We realise that covering all of these areas is not feasible within the scope of this proposal, and, accordingly this proposal will focus on:

- Optimal deployment of Golay waveform libraries, using coding of the sequence;
- Control of PRFs and CPIs with these limited libraries to achieve optimal performance using information metrics;
- A control-theoretic perspective on the radar resource allocation problem.

The key underlying concept in construction of the illumination schema regards the library element as not just a single pulse, but a sequence of pulses. Individual pulses considered will come from well-understood collections of waveforms such as Golays or chirps. Rather than building individual waveforms, what will be new is the focus on assembling these into collections that provide superior performance in a tracking context. We will develop these sequences of waveforms by taking a control theoretic perspective towards the design over multiple pulse repetition intervals (PRIs). The collections of waveforms will be kept as libraries for future optimization of tracking tasks.

1.2 Overview of the Project Work

During the project period, the research group in Melbourne led by the Principal Investigator Prof Bill Moran has made significant research effort to this project. This include the following achievements.

1. Published 7 refereed journal and 4 conference papers from the work related to the project;
2. Two technical reports [1, 2] for this project under the Grant No. FA2386-15-1-4066 were submitted to Asian Office of Aerospace Research & Development (AOARD). Prof Bill Moran has multiple visits to AFRL Dayton to present the project work.
3. Project manager Dr Seng Hong from AOARD visited the group (workshop) at RMIT University in Melbourne (2016);
4. Project technical manager Dr Braham Himed from AFRL has visited the group twice (2016 and 2017) to join the group research work briefing and discussion;

Next, we briefly summarise our AOARD project work carried out during May 2015—May 2017, which has been reported in [1, 2]. An update for recent work is given in the next section.

1.2.1 UAV Trajectory Scheduling [1]

(**Investigators:** Sofia Suvorova, Branko Ristic and Bill Moran with advice from Braham Himed)

The problem is to tracking a non-responsive target by a UAV using a Markov Decision Process (MDP) model. As part of this work package, a new tracker was developed to handle both clutter (modelled as a Poisson process) and either monostatic or bistatic measurements. Scheduling of the UAV platform is done to optimize the mutual information between the estimated target state (as provided by the tracker) and the measurement. We find a stationary (that is, time-independent) policy to optimize the trajectory of the platform according to this information measure. It is assumed that both target and the UAV platform have similar dynamical properties. Both the monostatic and bistatic (with a stationary source) measurements are considered. In both cases, it was found that the optimal trajectory for the platform involved the UAV platform(s) to close in on the target. This is not surprising, mutual information in the measurement is maximized by proximity of the platform to the target. As a result further simulations were done with a "guard range" to constrain the platform not to approach closer than a fixed distance from the target.

We are preparing a paper to be submitted to Fusion 2017.

1.2.2 Game Theoretic Formulation of Target Tracking [1]

(**Investigators:** Yangbo Yang, Xuezhi Wang, Tim Brown, and Bill Moran, with advice from Braham Himed)

In this case, both target and sensor have some sensing capability and the ability to manoeuvre to reduce the effectiveness of measurements by the each other. An extended Kalman Filter (EKF) tracker was implemented but the measure of effectiveness was complicated. Each of the platform and the target has a combined measure that is a convex combination of the each's mutual information between its estimated state of the other and its measurement, and the negative of this quantity (as estimated) for the other. Thus, depending on the relative weight attached to the two parts, each will attempt to maximize the mutual information in its measurement of the other, and minimize its estimate of the mutual information that the other has about it. The platform is assumed to have an active sensor, such as a radar, with SNR decreasing as the 4th power of distance, and the target a passive sensor, measuring just direction and amplitude of the platform's emissions. Scheduling is on an epoch-by-epoch basis; that is, no long term effects are taken into account, Results of simulations are presented for a range of emphases between the *curious* (high weighting of our measurement mutual information and low weighting of opponent mutual information) and the *paranoid* (low weighting of measurement mutual information and low weighting of opponent mutual information) possibilities for the parameters. This has led to some interesting dynamics that are the subject of continuing further study by the group.

A paper is under preparation. We have not yet decided the venue.

1.2.3 Passive Sensor Trajectory Optimisation [1]

(**Investigators:** Xuezhi Wang and Bill Moran)

In this work, tracking a moving target using two bearings-only sensors is considered. The underlying problem is to schedule the trajectories of the two sensors to minimise the track error. The measure of effectiveness used in scheduling is the determinant of the Fisher Information matrix of the measurement. Scheduling is done on a greedy basis, that is, the optimal is chosen at each time.

1.3 Radar Waveform Scheduling for Multiple Nonzero Doppler Target Detection [2]

(**Investigators:** Jiahua Zhu, Xuezhi Wang, Sofia Suvorova and Bill Moran)

Golay complementary waveforms, which constitute a pair A and B of time separated waveforms, appear to be ideal candidates in radar to generate high range resolution pulses for target detection. However, when A and B are transmitted in an alternating sequence, range-dependent sidelobes, artefacts of the processing, appear in the non-zero Doppler bins. This problem was addressed by several authors including Moran and Suvorova in earlier work, by careful reordering of the waveforms. These Doppler resilient Golay complementary waveforms yield a region of Doppler bins around the zero Doppler bin in which range sidelobes are very significantly reduced [3, 4]. More recently Dang *et. al.* in [5, 6] have used a Binomial design algorithm to filter the return in conjunction with the previously developed sequencing technique to produce further improvements in the reduction and clearing of range sidelobes near the zero Doppler bin. We have also reported last year that Suvorova *et. al.* in [7] a proposed algorithm that can achieve an enhanced SNR near the Doppler of a tracked non-zero Doppler target by transmitting Golay complementary waveforms using Reed-Muller sequences to provide the sequence order of the pairs.

In 2016, we continued to work on this topic, and specifically in extending the work of Suvorova *et al.* A signal processing procedure is proposed, which extends Suvorova's work [7] to include multiple targets with non-zero Doppler and add a nonlinear minimum operation processor to combine the outputs from both this algorithm and the Binomial design algorithm in the range-Doppler maps. Significant sidelope suppression has been observed.

1.4 Sensor Trajectory Optimisation [2]

(**Investigators:** Xuezhi Wang, Sofia Suvorova and Bill Moran)

Recall that in the technical report to AOARD on May 2016, our research in this project involves two scenarios:

1. **UAV trajectory scheduling:** tracking a target using a sensor on a moving UAV platform which obtains both range and azimuth measurements of the target;

2. **Passive sensor trajectory scheduling:** tracking a target using two cooperative bearings-only sensors with each on a moving UAV platform.

A greedy (one-step ahead) search algorithm is applied to compute the best sensor trajectory based on the stationary optimisation policies, which implies 1) for **UAV trajectory scheduling**, the velocity of the UAV platform depends only on target velocity; 2) for **Passive sensor trajectory scheduling**, the sensor platforms moves at a constant speed, while its directions are target state dependent. Both of these efforts have been reported in the technical report to AOARD in June 2016.

In this progress report, we describe the extension of the work on the second scenario, where we consider how to determine the right cost function for this two bearings-only sensor trajectory optimisation for tracking a moving target.

1.5 Game Theoretic Formulation of Target Tracking [2]

(**Investigators:** Yanbo Yang, Xuezhi Wang, Tim Brown and Bill Moran)

Commencing in early 2016, this work studies the dynamical behavior of a target-sensor system under a (fair) game theoretic formulation. While both target and sensor platform (UAV)

have identical maneuvering capabilities, their sensing capabilities are slightly different. Furthermore, the nature of "catch" and "escape" activities between the target-sensor pair leads to different optimisation policies which are adopted by greedy scheduling of their motions based on a combined cost. Mutual information based cost functions were implemented describing the sensor's knowledge of the target and its belief of the target's knowledge of the sensor, as well as corresponding combinations for with the roles of the sensor and target interchanged. Weighting parameters, $\lambda_{s,k}$ and $\lambda_{x,k}$ are used to combine these information metrics for each of the sensor and target respectivel. Our earlier work in [8] for characterising the uncertainties of sensor observation while tracking has assisted in the development of this work. In our simulations, several stationary motion patterns due to the variation of these parameters have been observed.

We are investigating and analysing the relations of between these stationary "catch" and "escape" patterns and the values of associated "belief" parameters. A journal paper for the project under this topic is in preparation.

2 Recent Work

Below we provide an update on the recent work (May 2017 – Dec 2017) related to the AOARD project under Grant No. FA2386-15-1-4066.

2.1 Radar waveform scheduling for the detection of multiple moving targets

(**Investigators:** Jiahua Zhu, Xuezhi Wang, Sofia Suvorova and Bill Moran)

This is an ongoing research under the topic of radar waveform scheduling for multiple moving target detection problem. Golay complementary waveforms can, in theory, yield radar returns of high range resolution with essentially zero sidelobes. In practice, with conventional deployment, while high signal-to-noise ratios can be achieved for static target detection, considerable range sidelobes are generated by target returns of nonzero Doppler causing unreliable detection.

Several signal processing techniques were proposed to improve radar detection performance in the detection scenarios involving multiple moving targets under the Golay complementary waveforms [9]. In this report period (May 2017 - December 2017), the work along this topic involves

1. Pointwise Addition versus Pointwise Minimisation Processor;
2. Detection probability analysis and target detection in sea clutter [10];
3. Sidelobe suppression in multi-static radar networks [11].

2.1.1 Alternative Signal Processing of Complementary Waveform Returns for Range Sidelobe Suppression

Reducing sidelobes for processing nonzero Doppler target returns under Golay complementary waveforms is important. While the pointwise minimum processor in our early work shows enhanced performance in the suppression of range sidelobes compared with existing approaches, it has a reduced detection probability for a target with location uncertainties. In this paper, we present an alternative processing method which combines the radar returns in two separated pairs of Golay complementary waveforms through a pointwise addition processor. Our simulation result shows that this alternative method has a similar performance to that of the pointwise minimum processor but results in an improved target detection probability.

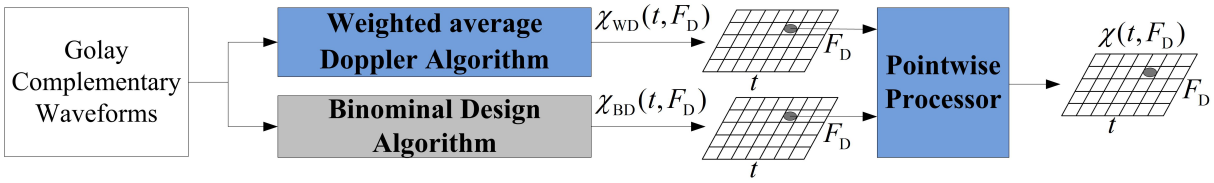

Figure 1: Illustration of the signal processing procedure: Pointwise processor = minimum operator → PMP; Pointwise processor = addition operator → PAP.

Golay Complementary Waveforms A Golay complementary waveform consists of two unimodular (± 1) sequences $x(l)$ and $y(l)$ of length L ($x(l)$ and $y(l)$ are called a Golay complementary pair, and details on their generation can be found in [24]). The time extent of each chip in the pair is T_{c} and the total time duration of each pair is LT_{c}. The autocorrelation of a Golay complementary pair satisfies $C_{\mathrm{x}}(k) + C_{\mathrm{y}}(k) = 2L\delta(k)$, $k = -(L-1), ..., (L-1)$, where $C_{\mathrm{x}}(k)$ and $C_{\mathrm{y}}(k)$ are the autocorrelation output of $x(l)$ and $y(l)$ at lag k respectively, and $\delta(k)$ is the Kronecker delta function. A baseband pulse $\Omega(t)$ with unit energy, i.e. $\int_{-T_{\mathrm{c}}/2}^{T_{\mathrm{c}}/2} |\Omega(t)|^2 \mathrm{d}t = 1$, is modulated on each chip interval by each of the Golay complementary pair, so that the transmitted sequences are expressed as $x(t) = \sum_{l=0}^{L-1} x(l)\Omega(t - lT_{\mathrm{c}})$, $y(t) = \sum_{l=0}^{L-1} y(l)\Omega(t - lT_{\mathrm{c}})$. A (P, Q) pulse train is used to determine which of $x(t)$ and $y(t)$ is transmitted in each pulse. Here $P = \{p(n)\}_{n=0}^{N-1}$ is a binary sequence, so that the transmitted signal is as

$$z_P(t) = \sum_{n=0}^{N-1} p(n)x(t - nT) + (1 - p(n))y(t - nT) \tag{1}$$

where T is the pulse repetition interval (PRI). The $(n+1)^{\mathrm{th}}$ pulse in $z_P(t)$ is $x(t)$ if $p(n) = 1$ and is $y(t)$ if $p(n) = 0$. The alternating sequence $P = \{0, 1, 0, 1, ...\}$ is the standard transmission order for Golay complementary waveforms. The sequence $Q = \{q(n)\}_{n=0}^{N-1}$ of positive real numbers is applied to the received signal to weight the returns. The pulse train for the matched filtering is

$$z_Q(t) = \sum_{n=0}^{N-1} q(n)[p(n)x(t - nT) + (1 - p(n))y(t - nT)] \tag{2}$$

The standard weighting sequence Q is an all 1 sequence.

According to [13], the ambiguity function of this filtered pulse train is

$$\chi_{PQ}(t, F_{\mathrm{D}}) = \int_{-\infty}^{+\infty} z_P(s) \exp(j2\pi F_{\mathrm{D}} s) z_Q^*(t - s)\mathrm{d}s \tag{3}$$

where the superscript "*" denotes complex conjugation.

As mentioned earler, Golay complementary waveforms, transmitted in standard order and matched filtered with the standard weighting sequence, produce enormous range sidelobes in nonzero Doppler bins, essentially increasing the false alarm rate for target detection, or correspondingly reducing detection rate. This problem is addressed by the PMP algorithm described below.

Pointwise Minimisation Procedure The PMP algorithm proposed previously [4] for range sidelobe suppression under Golay complementary waveforms is summarized in Fig. 9, where $\chi_{\mathrm{WD}}(t, F_{\mathrm{D}})$ and $\chi_{\mathrm{BD}}(t, F_{\mathrm{D}})$ are Delay-Doppler maps for the WD and BD algorithms, respectively, $\chi(t, F_{\mathrm{D}})$ being the final output from the pointwise processor. Specifically, in our early work [23], the "Pointwise Processor" in Fig. 9 represents the *pointwise minimization processor (PMP)*. We denote the final output of PMP by $\chi_{\mathrm{PMP}}(t, F_{\mathrm{D}})$. For the BD algorithm [5], P is the standard transmission order, and $Q = \alpha \times \{C_{N-1}^n\}_{n=0}^{N-1}$, where $\alpha = N/\sum_{n=0}^{N-1} C_{N-1}^n$, C_{N-1}^n represents the number of subsets of size n from a given set of size $N - 1$. For the WD algorithm [4],

while Q is the standard weighting sequence, P is calculated using the method in [14] to select the optimal transmission order to minimize range sidelobes near the average Doppler $\bar{f}_{\mathrm{d}}$ of the targets weighted by the associated target amplitudes

$$\bar{f}_{\mathrm{d}} = \begin{cases} \frac{\sum_{h=1}^{H} f_{\mathrm{d}_h}}{H} & \text{if all } A_h \text{ are the same,} \\ \frac{\sum_{h=1}^{H} (1-A_h) f_{\mathrm{d}_h}}{\sum_{h=1}^{H} (1-A_h)} & \text{otherwise.} \end{cases} \tag{4}$$

where H is the number of targets in the Delay-Doppler map, A_h and f_{d_h} are the normalized amplitude and Doppler of the h^{th} target respectively. Target Doppler can often be estimated in a separate process, e.g., the detection of a Doppler radar, or the prior Doppler predicted by a tracker using past detections ([15] Chs. 2.3.4).

A PMP is then employed to combine the outputs of the WD and BD algorithms:

$$\chi_{\mathrm{PMP}}(t, F_{\mathrm{D}}) = \min \left\{ \chi_{\mathrm{WD}}(t, F_{\mathrm{D}}), \chi_{\mathrm{BD}}(t, F_{\mathrm{D}}) \right\}. \tag{5}$$

The final result retains the large range sidelobe blanking area (the area where range sidelobes are less than -90dB) of the BD algorithm as well as the Doppler resolution given by the WD algorithm, at least theoretically. However, a drawback of PMP is that the radar cross section of the target, or the "effective detectable area" of target reflected by the Delay-Doppler resolution may be reduced in the final output when the underlying target has location uncertainties. The PAP is motivated by this consideration and is described next.

The Pointwise Addition Procedure To solve the drawback induced by the PMP, we propose a *pointwise addition processor (PAP)* to replace the PMP. Denoted by $\chi_{\mathrm{PAP}}(t, F_{\mathrm{D}})$, the final output of PAP is expressed as

$$\chi_{\mathrm{PAP}}(t, F_{\mathrm{D}}) = \mathrm{norm} \left\{ \chi_{\mathrm{WD}}(t, F_{\mathrm{D}}) + \chi_{\mathrm{BD}}(t, F_{\mathrm{D}}) \right\} \tag{6}$$

where "norm" is the normalization operation.

The operation of PAP and PMP are based on the same theory, that is under the assumption that the target is stable during the whole radar illumination period (the location and magnitude of the target are stationary in two Delay-Doppler maps), but the range sidelobes yielded are different. The use of PAP mitigates the reduction of the target detection probability caused by the nonlinear PMP, while maintaining a comparable range sidelobe blanking area and Delay-Doppler resolution similar to the PMP in theory.

In order to compare the performances of PAP and PMP, we use the *peak to peak-sidelobe ratio (PPSR)* in [15] as a measure. It is defined by

$$PPSR(F_{\mathrm{D}}) = \frac{|\chi(0,0)|^2}{\max\limits_{t \in S_{\mathrm{d}}} |\chi(t, F_{\mathrm{D}})|^2} \tag{7}$$

where S_{d} contains the delays where the range sidelobes are located. The PPSR measures the performance of range sidelobe suppression at a desired Doppler value, and in fact calculates the ratio of the energy of the peak in the ambiguity function (the target) to that of the largest range sidelobe at Doppler F_{D}. It can be expected that the PMP will produce a higher PPSR than PAP.

In the presence of a Swerling II target, the detection situation in the Delay-Doppler map, taking into account target location uncertainties, is illustrated in Fig. 2 [13]. Intuitively, while PMP can achieve a higher PPSR, it potentially results in a smaller effective radar cross section. On the other hand, the ambiguity function of PAP has a larger effective radar cross section at the cost of sacrificing Delay-Doppler resolution and PPSR. In other words, PAP actually

performs worse than PMP from the viewpoint of range sidelobe suppression and Delay-Doppler resolution for a Swerling II target, but obtains a larger effective radar cross section for the target (yielding higher target detection probability). Nevertheless, in the simulation result shown in Fig. 6, the reduced PPSR of PAP remains reasonably high in enabling identification of a target from sidelobes.

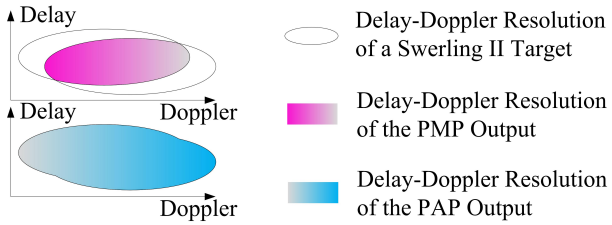

Figure 2: Comparison of radar cross sections for a target of Swerling II model under PMP and PAP algorithms.

Simulation and Discussions The performance of PAP is confirmed by simulation with the following parameters: radar carrier frequency $f_c = 1$GHz, bandwidth $B = 50$MHz, sampling rate $f_s = 2B$, PRI $T = 50\mu$s, pulse number $N = 2^5 = 32$. Golay complementary waveforms have, for each element of the pair, $L = 64$ chips of values ± 1 in chip interval $T_c = 0.1\mu$s. Each chip has $f_s \times T_c = 10$ sampling points.

As described in [4], the ambiguity functions of $\chi_{\mathrm{BD}}(t, F_{\mathrm{D}})$ and $\chi_{\mathrm{WD}}(t, F_{\mathrm{D}})$ are computed and divided into the following two parts

$$\begin{aligned}\chi_{\mathrm{BD}}(t, F_{\mathrm{D}}) &= \frac{1}{2}\sum_{k=-L+1}^{L-1}[C_{\mathrm{x}}(k) + C_{\mathrm{y}}(k)]\sum_{n=0}^{N-1} q_{\mathrm{BD}}(n)\xi_{nk} \\ &\quad - \frac{1}{2}\sum_{k=-L+1}^{L-1}[C_{\mathrm{x}}(k) - C_{\mathrm{y}}(k)]\sum_{n=0}^{N-1}(-1)^{p_{\mathrm{BD}}(n)} q_{\mathrm{BD}}(n)\xi_{nk} \\ &\triangleq G_{\mathrm{BD}}(t, F_{\mathrm{D}}) + S_{\mathrm{BD}}(t, F_{\mathrm{D}}) \qquad (8)\end{aligned}$$

$$\begin{aligned}\chi_{\mathrm{WD}}(t, F_{\mathrm{D}}) &= \frac{1}{2}\sum_{k=-L+1}^{L-1}[C_{\mathrm{x}}(k) + C_{\mathrm{y}}(k)]\sum_{n=0}^{N-1} q_{\mathrm{WD}}(n)\xi_{nk} \\ &\quad - \frac{1}{2}\sum_{k=-L+1}^{L-1}[C_{\mathrm{x}}(k) - C_{\mathrm{y}}(k)]\sum_{n=0}^{N-1}(-1)^{p_{\mathrm{WD}}(n)} q_{\mathrm{WD}}(n)\xi_{nk} \\ &\triangleq G_{\mathrm{WD}}(t, F_{\mathrm{D}}) + S_{\mathrm{WD}}(t, F_{\mathrm{D}}) \qquad (9)\end{aligned}$$

where $\xi_{nk} = \exp(j2\pi F_{\mathrm{D}} nT) C_\Omega(t - kT_c - nT)$.

Fig. 5 shows the ambiguity functions of the BD algorithm, WD algorithm, the PMP output and the PAP output, and slices across them at the zero-delay. Note that the first terms in (17) and (18) are contributed by the target return — corresponding to the peak of the ambiguity function, highlighted in the red rectangles in Fig. 5. The second terms represent the sidelobes induced by signal processing. The last row of Fig. 5 illustrates the output of PAP. It indicates that PAP has similar performance to PMP in terms of the scale of range sidelobe blanking area, as well as mainlobe width.

The PPSR plots for PAP and PMP are compared in Fig. 6. It is obvious that the PPSR curve of PMP is always higher than that of PAP within the Doppler interval $[0, \pi]$rad. Thus PAP generates larger range sidelobes than PMP, as shown in the Delay-Doppler maps. Nevertheless,

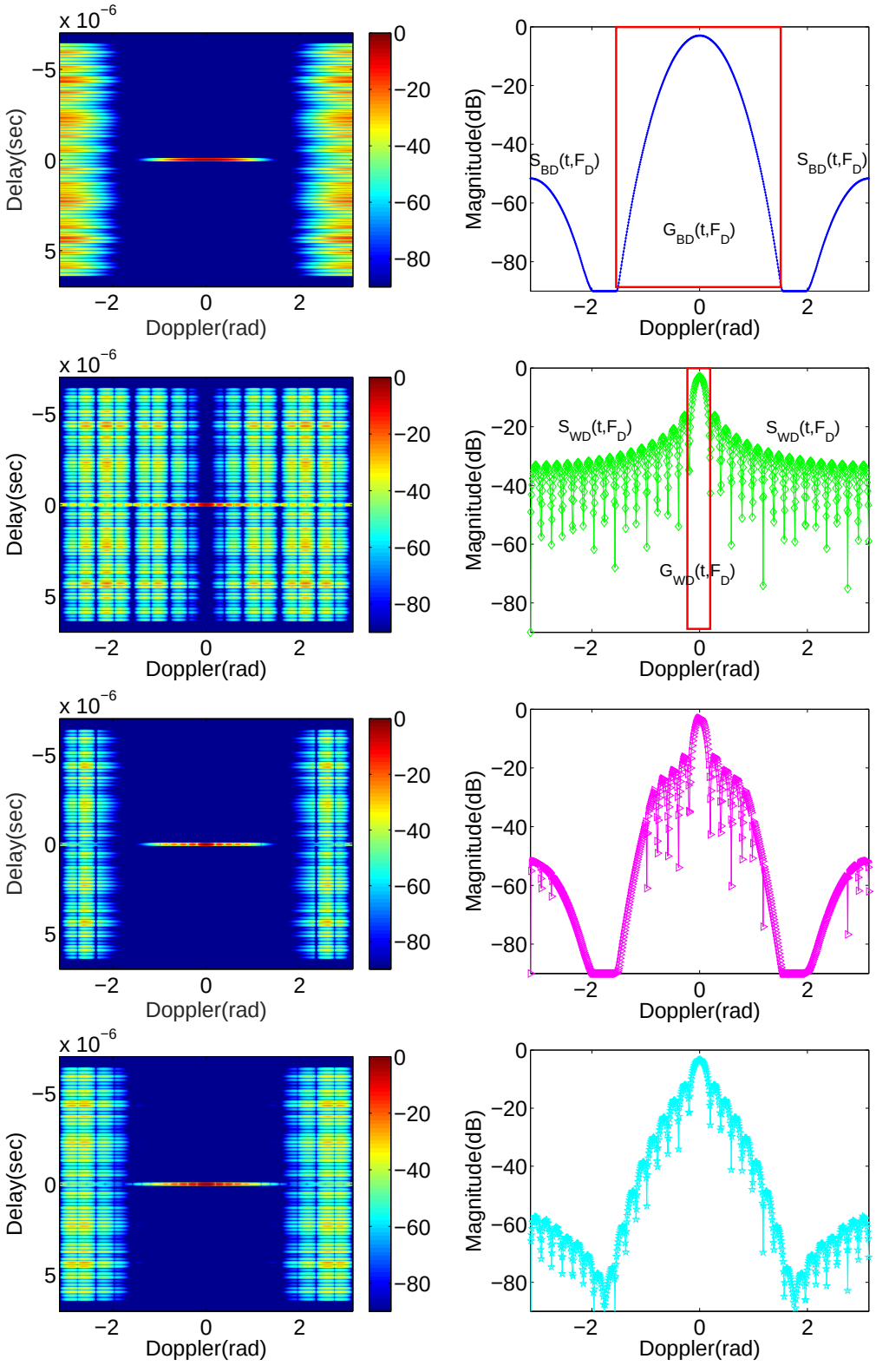

Figure 3: Plots of ambiguity functions $\chi_{\mathrm{BD}}(t, F_{\mathrm{D}})$, $\chi_{\mathrm{WD}}(t, F_{\mathrm{D}})$, $\chi_{\mathrm{PMP}}(t, F_{\mathrm{D}})$ and $\chi_{\mathrm{PAP}}(t, F_{\mathrm{D}})$ (column (a) from top to bottom) and the slices of them across the zero-delay (column (b) from top to bottom). (colorbar unit is dB)

the mean PPSR of the PAP output is greater than 95dB, which is high enough for differentiating the target returns from the range sidelobes.

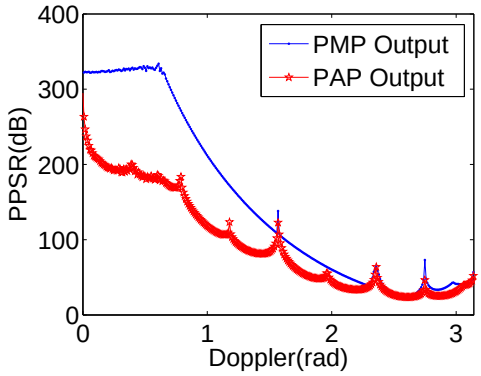

Figure 4: The comparison of the PPSR.

In summary, the analytical and simulation results confirm that the PAP performs no worse than the existing PMP but with an enhanced target detection probability, though a decrease of the PPSR values and Delay-Doppler resolution is observed through the ambiguity function. A journal paper in this work is currently in preparation.

2.1.2 Detection of Moving Targets in Sea Clutter Using Complementary Waveforms

Work of Pezeshki, Calderbank and others [3, 4] has shown that choice of transmission order of Golay complementary waveforms in radar pulse trains can significantly improve Doppler resilience in detecting nonzero Doppler targets. For multiple targets a Weighted average Doppler (WD) algorithm [16] based on our earlier work has been shown to provide improvements. In this work, we demonstrate that the Weighted Sidelobe Minimization procedure, developed in our recent work (see [9] for more detail) that combines the outputs of WD and the existing Binominal Design algorithms for ordering transmitted complementary waveform sequences using a point-wise minimization process (PMP), is also effective for the elimination of false target returns arising from sea clutter. A detailed analysis based on a Swerling II target model in terms of target detection probability is presented to validate the use of PMP. Our validation is strengthened by numerical simulations for both fixed and randomized scenarios.

The signal processing procedure The *Weighted Sidelobe Minimization (WSM) procedure* for Golay complementary waveforms [16] in our work is illustrated in Figure 9, where the radar returns are contaminated by sea clutter and noise, $\chi_{\mathrm{WD}}(t, F_{\mathrm{D}})$ and $\chi_{\mathrm{BD}}(t, F_{\mathrm{D}})$ are the Delay-Doppler maps for the Weighted average Doppler (WD) and BD algorithms respectively, operating in different transmission periods, and $\chi(t, F_{\mathrm{D}})$ is the final output Delay-Doppler map.

Technical summary Practical radar returns may contain the following uncertainties that influence target detection probability:

(1) Target return fluctuations caused by target micro-motion, modelled by the Swerling II target model, may vary the Delay-Doppler resolution of the target after the PMP and cause missed detections when fluctuations are significant;

(2) Sea clutter with potentially larger magnitude than the detection threshold may induce false alarm detection.

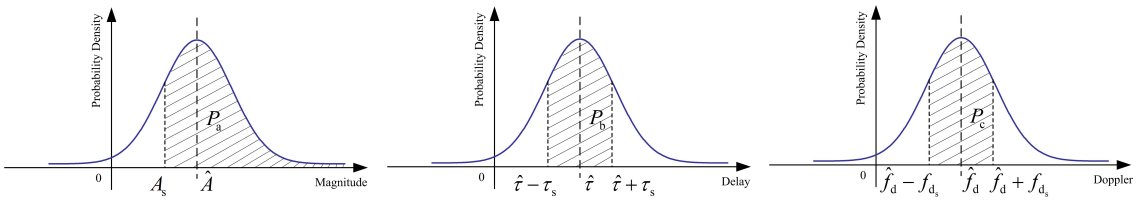

(a) (b) (c)

Figure 5: The relationship between the PDFs of three fluctuations in Swerling II target model and their boundaries.

In this work, we analyse the target detection probability under the signal procedure illustrated in Fig. 9 via an example of target detection in the presence of sea clutter, where a Swerling II target model is used for modeling the fluctuation of the underlying target return. Sea clutter is modeled as a uniform point process over the surveillance window in our following simulations with the occurrence density satisfying a Poisson distribution,

$$P(X|\lambda) = \frac{\lambda^X}{X!}e^{-\lambda} \tag{10}$$

where the parameter X and λ represent the actual and average number of false target-like sea clutter peaks appearing in the Delay-Doppler map.

Target Detection Probability The fluctuations of a Swerling II target comprise three independent fluctuations — the magnitude fluctuation (or RCS fluctuation), the delay fluctuation and the Doppler fluctuation, respectively. In the far field detection scene, they can be approximated by independent and identically distributed (IID) Guassian distributions [17] — $\mathcal{N}(\hat{A}, \sigma_{\mathrm{A}}^2)$, $\mathcal{N}(\hat{\tau}, \sigma_{\mathrm{T}}^2)$ and $\mathcal{N}(\hat{f}_{\mathrm{d}}, \sigma_{\mathrm{D}}^2)$, where $\hat{A}$, $\hat{\tau}$ and $\hat{f}_{\mathrm{d}}$ are the estimated (mean) values of the target magnitude, delay and Doppler, as can be obtained from a tracker; σ_{A}^2, σ_{T}^2 and σ_{D}^2 are their variances.

The worst acceptable case to maintain target detectability is that the magnitude of a target (though it is reduced) is still higher than the magnitude of a maximum sidelobe A_{s} (this is the detection threshold and assumed known in our simulation) after the PMP. For illustration purposes, we cut an elliptical cross section of the AF at height A_{s} around the peak associated with the target. This has delay and Doppler semi-axis τ_{s} and $f_{\mathrm{d_s}}$ representing feasible boundaries of delay and Doppler fluctuations. The relationship between the PDFs of these three fluctuations and their boundaries are illustrated in Figure 5.

The integrals of the shadow areas in Figure 5 represent the probabilities that the fluctuations are within the boundaries, and we denote these three probabilities by P_{a}, P_{b} and P_{c} ($0 < P_{\mathrm{a}}, P_{\mathrm{b}}, P_{\mathrm{c}} < 1$), respectively. Using the properties of the Gaussian distribution [17], we calculate P_{a}, P_{b} and P_{c}:

$$P_{\mathrm{a}} = \int_a^{+\infty} \frac{1}{\sqrt{2\pi}} \exp\left(-\frac{1}{2}A^2\right) \mathrm{d}A, \tag{11}$$

$$P_{\mathrm{b}} = \int_{b_1}^{b_2} \frac{1}{\sqrt{2\pi}} \exp\left(-\frac{1}{2}\tau^2\right) \mathrm{d}\tau \tag{12}$$

$$P_{\mathrm{c}} = \int_{c_1}^{c_2} \frac{1}{\sqrt{2\pi}} \exp\left(-\frac{1}{2}f_{\mathrm{d}}^2\right) \mathrm{d}f_{\mathrm{d}} \tag{13}$$

where $a = (A_{\mathrm{s}} - \hat{A})/\sigma_{\mathrm{A}}$, $b_1 = -\tau_{\mathrm{s}}/\sigma_{\mathrm{T}}$, $b_2 = \tau_{\mathrm{s}}/\sigma_{\mathrm{T}}$, $c_1 = -f_{\mathrm{d_s}}/\sigma_{\mathrm{D}}$, $c_2 = f_{\mathrm{d_s}}/\sigma_{\mathrm{D}}$.

Since the three fluctuations are IID Guassian distribution, the target detection probability P_{D} after PMP is

$$P_{\mathrm{D}} = P_{\mathrm{a}} \times P_{\mathrm{b}} \times P_{\mathrm{c}}. \tag{14}$$

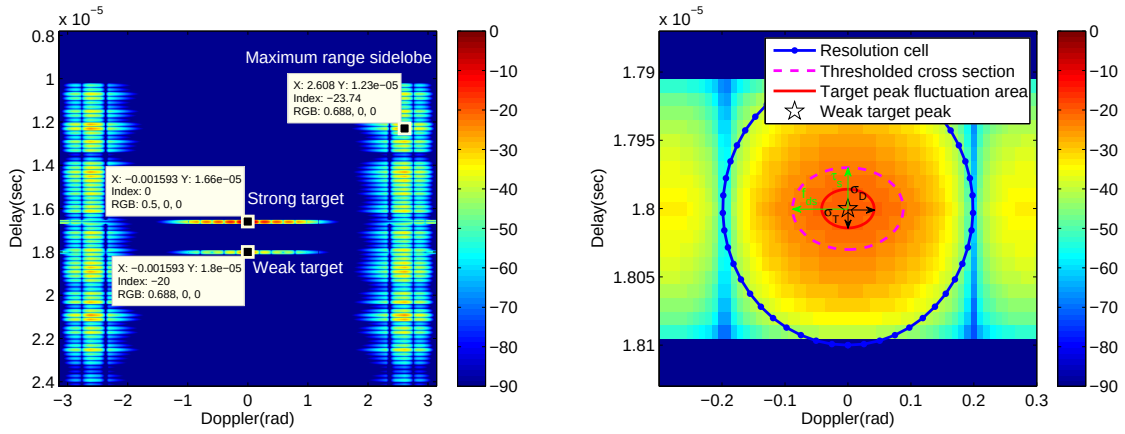

(a) (b)

Figure 6: (a) Illustration output result of $\chi(t, F_{\mathrm{D}})$; (b) a magnified version around the weak target. (the unit of colorbar is dB, illustration parameters are given in *Simulation result discussion*, except bandwidth $B = 50$MHz for better visual effect)

For a given P_{D}, the corresponding σ_{A}, σ_{T} and σ_{D} become tolerable fluctuation standard deviations and σ_{T} and σ_{D} shape a target peak fluctuation area in the Delay-Doppler map (it achieves maximum size when $P_{\mathrm{a}} = P_{\mathrm{b}} = P_{\mathrm{c}}$). Therefore, the fluctuation boundary conditions of a Swerling II target under a given detection probability are computable.

Example: Figure 6(a) is a sample result for $\chi(t, F_{\mathrm{D}})$ with a 0dB strong target and a -20dB weak target present (without sea clutter and noise), in which the maximum range sidelobe value is measured as -23.74dB from the figure. To detect the weak target with as little influence from sidelobes as possible, the detection threshold is chosen to be at least -23dB here. In this case, the cross section of the weak target at the threshold corresponding to τ_{s} and $f_{\mathrm{d_s}}$ gives semi-axes of 0.03μs and 0.088rad (or 4.5m and 42.02m/s as feasible boundaries of range and velocity fluctuations) as shown in Figure 6(b). If we require $P_{\mathrm{D}} = 0.9$, then $P_{\mathrm{a}} = P_{\mathrm{b}} = P_{\mathrm{c}} = 0.9655$, and σ_{A}, σ_{T}, σ_{D} are 0.2747, 0.0142μs and 0.0416rad, respectively. The allowable fluctuation area for the underlying target peak is shown as the red ellipse in Figure 6(b). On the other hand, the semi-axes of the target resolution cell in delay and Doppler are measured as 0.1μs and 0.1988rad, respectively. The tolerable magnitude of fluctuation relative to the original magnitude of the target is about 27.47%, and the tolerable delay and Doppler fluctuation of target peak to the resolution cell of target are about 14.20% and 20.93%, respectively. This the example highlights the conditions for detecting a Swerling II target under the WSM procedure. The determination of actual sidelobes in practice requires further study.

Simulation result discussion Simulations for the detection of 5 targets with various radar return strengths in the presence of sea clutter is performed with both fixed and randomised target locations where all targets are simulated using a Swerling II target model. Radar carrier frequency is assumed to be $f_{\mathrm{c}} = 1$GHz, bandwidth $B = 5$MHz, sampling rate is $f_{\mathrm{s}} = 2B$, PRI is $T = 50$ μs, number of pulses $N = 2^5 = 32$. For the Golay complementary waveforms, the number of chips is $L = 64$ with values ± 1 and the chip interval is $T_{\mathrm{c}} = 0.1\mu$s. The resolution cell in the Delay-Doppler map is $0.1\mu\mathrm{s} \times 0.001\pi\mathrm{rad}$. Identical carrier frequency, bandwidth, sampling rate, pulse length and PRI are set for the LFM waveform for comparison with the complementary waveforms.

Simulation results shown in Figure 7 indicate that the WSM procedure outperforms the other four results for detection performance in the presence of sea clutter. As the number of targets in the Delay-Doppler map increases, the detection performance of all approaches deteriorate. This

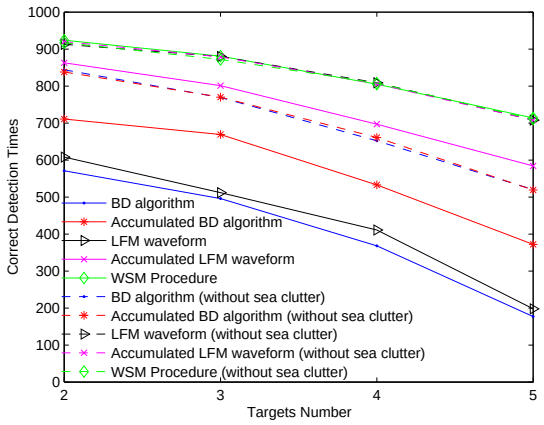

Figure 7: Statistical simulation results of correct detection times using BD algorithm, Accumulated BD algorithm, LFM waveform, Accumulated LFM waveform and WSM procedure with/without the influence of sea clutter.

is because range sidelobes increase as more targets enter the scene. In addition, the results for the (Accumulated) LFM waveform appear to have more correct detections than the (Accumulated) BD algorithm, and can achieve almost identical detection performances as the WSM procedure in the absence of sea clutter.

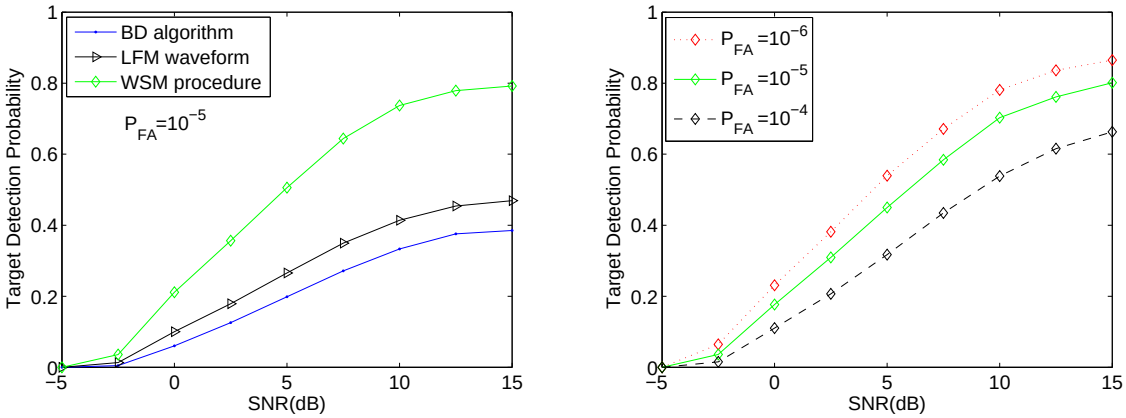

(a) (b)

Figure 8: (a) Approaches comparison: target detection probabilities as a function of SNR with $P_{\mathrm{FA}} = 10^{-5}$ as a parameter; (b) Target detection probabilities of WSM procedure in different false alarm rates.

Fig. 8 illustrates the target detection probabilities of the WSM procedure, the LFM waveform and the BD algorithm under several different SNR values and false alarm rates. It shows that the WSM procedure has similar target detection probability to the other two approaches when SNR is low. This is because the targets are almost submerged in noise and undetectable; while it is better than others under high SNR, as discussed earlier. On the other hand, since the false alarm rate is raised by increasing the occurrence density of sea clutter (which actually decreases the signal-to-clutter ratio) in this simulation, it is reasonable to expect a fall in target detection probabilities from using the WSM procedure when enhancing the false alarm rates, and this phenomenon will occur similarly in the other approaches.

Note that this work is published and more details can be found in [10].

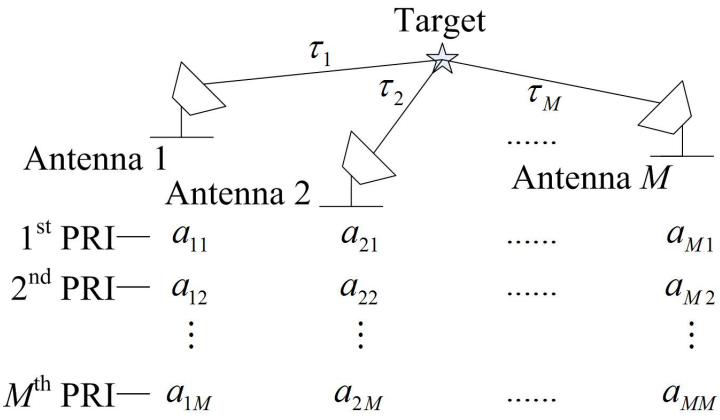

Figure 9: The schematic figure of the radar detection scenario.

2.1.3 Sidelobe suppression in multi-static radar networks

Background One of the key issues of distributed multistatic radar is to transmit distinguishable waveforms and obtain high signal-to-noise ratio (SNR) at the receivers. Deployed waveforms like the linear frequency modulated (LFM) waveform [19], orthogonal frequency division multiplexing (OFDM) waveforms [20], or a combination usage of them, though able to obtain an impulse-like output through matched filtering, need well separated carrier frequencies for individual antennas to reduce cross-antenna interference in the matched filtering, necessitating a large bandwidth for the centralized signal processing.

In this work, an alternative waveform scheme built on mutually orthogonal complementary sets is proposed for a distributed multistatic radar. Signal separation between antennas is established through the complementary sets, which reduce the bandwidth requirement as an identical carrier frequency is used in a centralized signal processing environment. We give a theoretical analysis of the influence of carrier frequencies and phases on range sidelobe suppression using complementary sets, validated by our simulations of multiple targets illumination. This varies from Searle *et al.* [21, 22], in that we avoid nonlinear processing of the complementary sets. Such processing can sometimes cause loss of target information [18].

Radar System based on Mutually Orthogonal Complementary Sets The Δ' matrix is used to compose the transmitted waveforms for a distributed multistatic radar system with antennas $1, 2, ..., m, ..., M$ that can both transmit and receive signals. Consider a static point target illuminated by the radar system as shown in Fig. 9, where τ_1 to τ_M are the round-trip delay values of the target to each antenna. Antenna m transmits the sequence a_{mp} in the pth ($p = 1, 2, ..., M$) pulse repetition interval (PRI) and receives echoes from all antennas; that is, the radar returns delayed versions of $[a_{1p}, \cdots, a_{Mp}]$. The complementary sets on each antenna are modulated by a baseband pulse $\Omega(t)$, yielding the following time domain waveforms:

$$a_{mp}(t) = \sum_{l=0}^{L-1} a_{mp}(l)\Omega(t - lT_c), \tag{15}$$

where $\int_{-T_c/2}^{T_c/2} |\Omega(t)|^2 \mathrm{d}t = 1$. Ideally, $\Omega(t)$ is a rectangle pulse, and this is used in our simulations for simplicity, but in a real system the rectangle pulse would typically be replaced by another pulse shape, such as a raised cosine or Gaussian pulse to reduce the bandwidth requirement.

$a_{mp}(t)$ is modulated by the carrier frequency f_{c_m} and a phase ϕ_m of antenna m to be the transmission waveforms $a_{mp}(t)e^{j2\pi f_{c_m}(t+\phi_m)}$. The signal received by antenna m in the pth PRI is

$$y_{mp}(t) = \sum_{i=1}^{M} a_{ip}\left(t - \frac{\tau_i + \tau_m}{2}\right) e^{j2\pi f_{c_i}\left(t - \frac{\tau_i+\tau_m}{2} + \phi_i\right)}, \tag{16}$$

and the output of antenna m for the pth PRI after demodulation with $e^{-j2\pi f_{c_m}(t+\phi_m)}$ and match filtering with $a_{mp}(t)$ is

$$z_{mp}(t) = \sum_{k=-L+1}^{L-1} \left\{ y_{mp}(t)e^{-j2\pi f_{c_m}(t+\phi_m)} \left(y_{mp}(t)e^{-j2\pi f_{c_m}(t+\phi_m)} \right)^* \right\}, \tag{17}$$

where the superscript "*" denotes complex conjugation. Summing the results over all M PRIs, we obtain a final output of antenna m:

$$z_m(t) = \sum_{k=-L+1}^{L-1} \left\{ \sum_{p=1}^{M} y_{mp}(t)e^{-j2\pi f_{c_m}(t+\phi_m)} \left(y_{mp}(t)e^{-j2\pi f_{c_m}(t+\phi_m)} \right)^* \right\}. \tag{18}$$

Influence of Carrier Frequencies and Phases As mentioned before, f_{c_m} often varies across antennas for traditional waveforms like LFM waveform in order to guarantee orthogonality. This requires wide system bandwidth on demodulation. Additionally the different carrier dependent phases ϕ_m may also complicate the post-processing of radar returns (e.g. may decrease the output of coherent integration). However, the transmission of complementary sets with identical carrier frequency for all antennas, i.e. $f_{c_m} = f_c$ results in (18) becoming

$$z_m(t) = \sum_{i=1}^{M} \sum_{k=-L+1}^{L-1} \left\{ \sum_{p=1}^{M} C_{a_{mp},a_{ip}} \left(k - \frac{\tau_i + \tau_m}{2} \right) C_\Omega(t - kT_c)e^{-j2\pi f_c \left(\frac{\tau_m+\tau_i}{2} + \phi_m - \phi_i \right)} \right\}, \tag{19}$$

where C_Ω denotes the autocorrelation of the baseband pulse and

$$\sum_{p=1}^{M} C_{a_{mp},a_{ip}} \left(k - \frac{\tau_i + \tau_m}{2} \right) = \begin{cases} ML\delta(k - \tau_m) & i = m, \\ 0 & i \neq m. \end{cases} \tag{20}$$

As a consequence, the complementary sets achieve an impulse output with a single carrier and reduced receiver bandwidth requirements. In addition, at least in theory, the phase item $\phi_m - \phi_i$ does not influence the level of range sidelobes.

Based on previous discussions, the following **remarks** can be made:

a. Theoretically, complementary sets are free of cross-antenna interference as well as range sidelobes (induced by the cross terms of cross-correlation) when an identical carrier frequency is used for all antennas and the results are not influenced by the phase differences between antenna carriers. In this case, the radar has an equivalent pulse width of $2T_c$.

b. Compared to conventional LFM or OFDM waveforms, this alternative scheme reduces the bandwidth requirement of the centralized radar signal processing system at the cost of increased radar illumination time (needs more accumulation of pulses) for the same pulse width and sampling rate.

c. Remark **a.** will not hold for complementary sets if carrier frequency variation across antennas is large.

Our simulation shows that under identical carrier frequency across antennas, phase differences and/or small frequency drift or jitter cause little effect to the output SNR for all antennas, while increased range sidelobes arise if antennas are working at significantly different carrier frequencies. The interested readers may referred to [11] for more detail.

2.2 Experimental Analysis of a Game-Theoretic Formulation of Target Tracking

(Investigators: Y.Yang, B. Moran, X. Wang, T. Brown, S. Williams and Q. Pan)

2.2.1 Summary

In this work, optimal trajectories for two platforms with similar dynamics are calculated using a game theoretic formulation. Each platform makes noisy observations of the kinematic state of the other. The objective of each is to maximise observable information about the other while minimising the information the other is able to acquire about it. That is to say, each platform maximises the mutual information between the expected future measurement of the opposing platform and the current likelihood of the state whilst minimising the estimated mutual information between potential measurements of itself by the other and its actual state. The multi-objective optimisation problem for each platform is converted to a single optimisation using Pareto parameters to weigh the relative importance of the two information measures. The relationship between the two Pareto parameters, and different initial track initialisations is investigated. Remarkably this complex coupled system of two platforms exhibits, for suitably chosen values of the Pareto parameters, interesting cyclical behaviors that are worthy of further exploration.

2.2.2 Update

Most of the work has been reported in our previous reports [1, 2]. During the current report period, we have concentrated to work on two folds. First, effort was made toward to a journal paper by an extended analysis and discussion on the simulation results reported previously. The manuscript has been submitted to IEEE transactions on Signal Processing and is under review. Second, Bill Moran *et. al.* have done preliminary work in information geometry with respect to a multi-agent measurement system to highlight the importance of sensor trajectory planning, in particular, the sensor system involving multiple UAVs with limited observabilities. A while paper titled "Trajectory planning with Radar" was reported to AFRL [33].

2.3 Cooperative Sensing with Passive Mobile Sensors for Target Tracking

(Investigators: X. Wang, B. Ristic, B. Himed and B. Moran)

This is an ongoing work in which we look into the problem of tracking a 2D moving target with two bearing-only mobile sensors. Since the performance of such a tracking system is correlated with the states of these sensors [31], the sensor trajectory optimisation plays a significant role in the tracking system. In the latest, two statistical reward functions, namely, the Expected Rényi Divergence and the Determinant of Fisher Information Matrix which are used for sensor trajectory optimisation are analysed. While both of them can be implemented in closed-forms, practically, they can only be evaluated through approximation. Our analysis shows that the Expected Rényi Divergence is not suitable for this sensor trajectory scheduling problem because the cross correlation between sensor states is weakened significantly by linearization. In fact, we observe that the expected Rényi Divergence has similar performance to the trace of the Fisher information matrix. We demonstrate this failing using methods from information geometry. Simulation comparison based on the example of a non-cooperative target tracking using two cooperative bearing-only sensors is presented.

Some early work was reported in [2] and here we will only update those which are yet to be reported. The main result was presented in Fusion 2017 international conference [27]. Based on the work described below, we are preparing a journal paper.

2.3.1 Geometric interpretation on reward function

In [2], we reported that using the Expected Rényi Divergence as a reward function in the sensor trajectory optimisation results in a poor performance than using the Determinant of Fisher Information Matrix. In this work, we further demonstrate this performance difference using information geometry. It is well known that the Fisher information matrix can be used as a metric tensor defining a Riemannian manifold, called statistical manifold [28]. Therefore, the Riemannian geometry is used to describe statistical problems in terms of various connections of interest using the one-one correspondence between the statistical parameter model and Riemannian manifold. For example, the Fisher information distance defined in the statistical manifold can be used to compare parameterised distributions.

For the problem at hand, the family of probability distributions $S = \{p(\boldsymbol{\beta}|\mathbf{x})\}$, parameterised in the target location space $\mathbf{x} \in \mathbb{R}^2$, forms a 2D statistical manifold where $\mathbf{x}$ plays the role of a coordinate system of S. The Fisher information distance (FID) between $p(\boldsymbol{\beta}|\mathbf{x}(t_1))$ and $p(\boldsymbol{\beta}|\mathbf{x}(t_2))$ is defined as the integral along the curve $\mathbf{x}(t)$

$$\mathcal{D}_F\big(\mathbf{x}(t_1),\, \mathbf{x}(t_2)\big) \triangleq \min_{\mathbf{x}} \int_{t_1}^{t_2} \left(\sqrt{\left(\frac{d\mathbf{x}(t)}{dt}\right)^T \boldsymbol{G}\big(\mathbf{x}(t)\big) \left(\frac{d\mathbf{x}(t)}{dt}\right)} \right) dt, \tag{21}$$

which signifies the shortest geodesic in the Riemannian (statistical) manifold. Using local coordinates on the statistical manifold, the geodesic equations are given by the Euler-Lagrange equations as [28]

$$\frac{d^2 \mathrm{x}_l}{dt^2} + \sum_{i=1}^{n} \sum_{j=1}^{n} \Gamma_{ij}^{k} \frac{d\mathrm{x}_i}{dt} \frac{d\mathrm{x}_j}{dt} = 0, \qquad l = 1, 2.\ \ n = 2. \tag{22}$$

For convenience, we use the subscript i of $\mathbf{x}$ to represent its ith component and thus $\mathbf{x}_i,\ i = 1, 2$ are the coordinates of the curve $\mathbf{x}(t)$, $\Gamma_{ij}^{l},\ i, j = 1, 2$ are the *Christoffel symbols of the second kind* and are defined as Riemannian connection coefficients,

$$\Gamma_{ij}^{l} = \frac{1}{2} \sum_{k=1}^{2} g^{lk} \left(\frac{\partial g_{ik}}{\partial \mathbf{x}_j} + \frac{\partial g_{jk}}{\partial \mathbf{x}_i} - \frac{\partial g_{ij}}{\partial \mathbf{x}_k} \right), \quad i, j, l = 1, 2. \tag{23}$$

where $[g^{lk}]$ signifies the inverse of $\boldsymbol{G} = [g_{lk}]$ and Einstein notation for summation is used.

The geodesic equations in (22) are ordinary differential equations for the coordinates $\mathbf{x}_i,\ i = 1, 2$. A unique solution $\mathbf{x}(t)$ can be found for given initial conditions $\mathbf{x}(0)$ and $\dot{\mathbf{x}}$, which is analogous to an initial position $\mathbf{x}(0)$ and the "speed" $\boldsymbol{\nu} \in \boldsymbol{\mathcal{T}}_{\mathbf{x}} S$ in the sense of the classical mechanics, where $\boldsymbol{\mathcal{T}}_{\mathbf{x}}$ denotes the tangent vector of S at $\mathbf{x}$.

Assume that a geodesic is projected onto the parameter space $\mathbb{R}^2$ with a starting point $\mathbf{x}(0)$ and a tangent vector $\boldsymbol{\nu}$. The exponential map of the starting point is then defined as [29]

$$\exp_{\boldsymbol{\nu}} [\mathbf{x}(0)] \triangleq \boldsymbol{\Psi}\big(1;\, \mathbf{x}(0),\, \boldsymbol{\nu}\big). \tag{24}$$

where the notation $\boldsymbol{\Psi}\big(t;\, \mathbf{x}(0),\, \boldsymbol{\nu}\big)$ is used to signify a geodesic with a starting point $\mathbf{x}(0)$, a tangent vector $\boldsymbol{\nu}$ and end point $\mathbf{x}(t)$.

It can be shown that the length along the geodesic between $\mathbf{x}(0)$ and $\boldsymbol{\Psi}\big(1;\, \mathbf{x}(0),\, \boldsymbol{\nu}\big)$ is $|\boldsymbol{\nu}|$ [29, 32]. Thus, for a fixed $\boldsymbol{\nu}$ the plot of geodesics along all directions at $\mathbf{x}$ visualizes an FID circle centered at $\mathbf{x}$ in S. Intuitively, the projection of such a circle from statistical manifold to the parameter space characterises the capability of the underlying sensor. So, in addition to the Determinant of FIM, the FID circle projected in parameter space will be used to assess the performance of a statistical reward function.

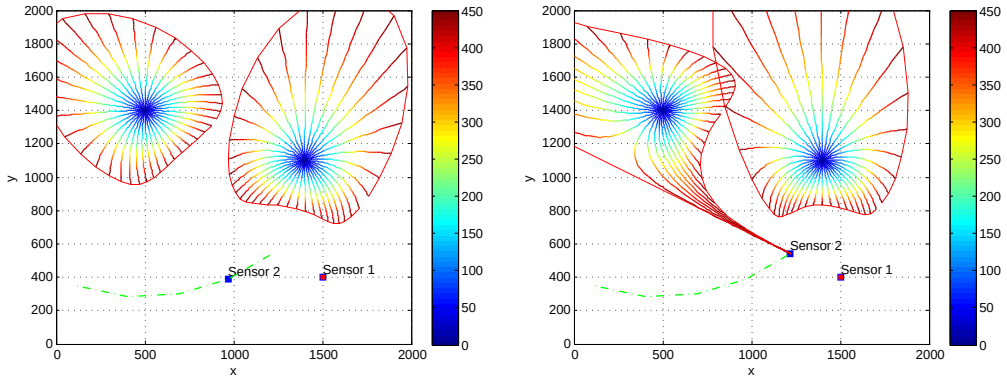

(a) (b)

Figure 10: Illustration of the circles of statistical manifold spanned by FIM for given sensor locations (a) Sensor 1 is at (1500,400) and Sensor 2 (973, 387). (b) Sensor 1 is at (1500,400) and Sensor 2 moved to (1219,544) in a circle around the target on the left.

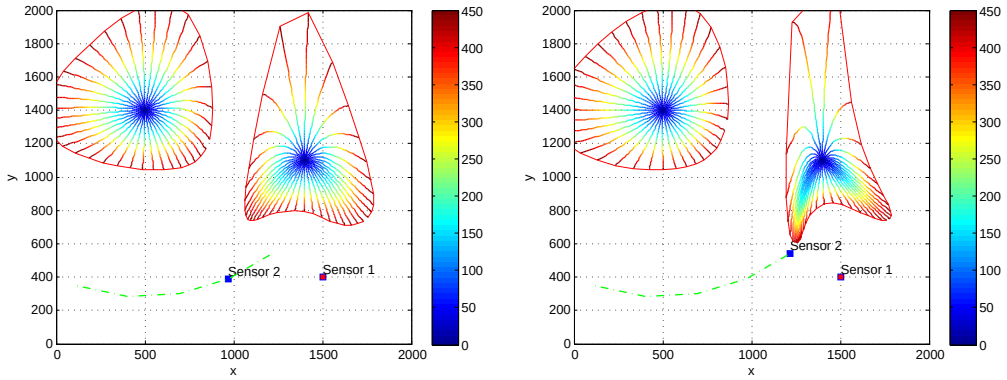

(a) (b)

Figure 11: Illustration of the circles of statistical manifold spanned by the FIM with constant valued off-diagonal elements for given sensor locations (a) Sensor 1 is at (1500,400) and Sensor 2 (973, 387). (b) Sensor 1 is at (1500,400) and Sensor 2 moved to (1219,544) in a circle around the target on the left.

To highlight the difference between the two statistical reward functions in question, we design the scenario where two fixed targets are observed by the two bearing-only sensors. The same parameterisations are used to compare the changes of Fisher information distance circles before and after the Sensor 2 moves in a circle around one target in the statistical manifolds spanned by the Fisher information matrices with and without taking into account the off-diagonal elements, respectively.

From the Fig. 10(a) to Fig.10(b), the FID circle around the target on the left has significant change in the statistical manifold spanned by the FIM as the Sensor 2 moves in a circle around that target. However, if the off-diagonal elements of FIM are ignored (or keeping constant), the trace of the resulting FIM is identical to that of the original. In the statistical manifold spanned by such a FIM there is no change to the FID circle centered at the target on the left as the Sensor 2 moves around the left target in circle as shown in Figures 10 (a) and (b). This result indicates that the Fisher information will not be fully explored if trace rather than determinant of the FIM is used as a statistical reward function. The Expected Rényi Divergence performs similar to the Trace of FIM.

2.3.2 Simulation example

We illustrate the significance of sensor scheduling using an example of tracking a maneuvering target by two bearing-only sensors. Target motion follows a hidden Markov process which contains the states of a left turn (-5^o), a right turn (5^o) and straightline (0^o) and it moving at a constant speed of 10m/s. The initial target state is $\mathbf{x}_0 = [600, 560, 10 * \cos(30^o), 10 * \sin(30^o)]'$. The scenario can be viewed in Fig. 12. In the first 50 of a total of 100 scans, the target is in left turn state and it turns into the right turn state in the rest of scans. Initially, the two bearing-only sensors are moving at a constant speed of 10m/s from the locations $S_1 = (1900, 560)$m and $S_2 = (1950, 560)$m heading in the directions 0^o and 60^o, respectively. They acquire bearing measurement of the target at a sampling rate of T=5s. During each scan, they will be steered to one of 5 directions with respect to their current headings according to the trajectory optimisation decision. The 5 directions are $-90^o, -45^o, 0^o, 45^o$ and 90^o.

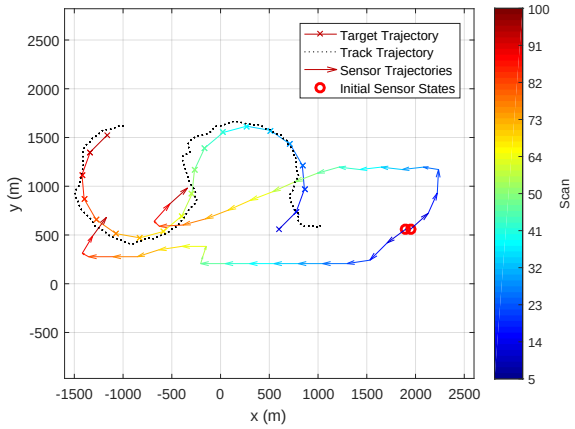

Figure 12: Illustration of the estimated target trajectory and the motion trajectories of the two bearing-only sensors optimised under DetFIM plotted from a single run, along with target ground truth trajectory.

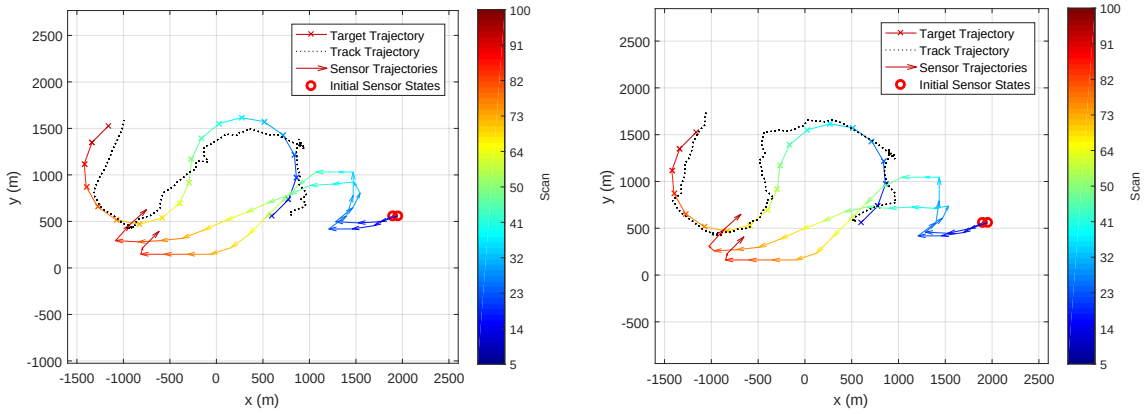

Figure 13: Estimated target trajectories with ground truth trajectory and the motion trajectories of the two bearing-only sensors optimised under (a) ExpReward; (b) TrFIM, plotted from a single run.

Therefore, for a N-Step ahead decision process, the number of action hypotheses yielded for the two cooperative sensors are $(5^2)^N$. For example, the number of action hypotheses for $N = 1$

is $5^2 = 25$ and for $N = 3$ is $(5^2)^3 = 15625$.

In practice, the maximum number of hypothesis histories allowed to steer future measurement at each epoch is constrained by a fixed number "MaxH" to provide a feasible computational overhead for real-time operation. In our simulation, we set MaxH = 1000 and under this constraint, it is found that the track error difference between $N > 3$ and $N = 3$ is negligible. Therefore, in the performance comparison versus Monte Carlo runs, we only consider $N \leq 3$.

An EKF tracker [30] is implemented to estimate the posterior density of target state from the target bearing measurements taken by the two sensors. We assume that the target bearing measurements are corrupted with a Gaussian noise of zero-mean with standard deviation 2^o.

Fig. 12, Fig. 13 (a) and Fig. 13 (b) show the typical trajectories of the two bearing-only sensors in the target tracking experiment under the Determinant of FIM (DetFIM), the Expected Rényi Divergence (ExpReward) and the Trace of FIM (TrFIM), respectively. By maximising DetFIM, the two sensors move in a way such that the angle formed by sensor 1, target, sensor 2 is approximately $\pi/2$ while approaching the target. So, the measurements taken by the two sensors along these computed trajectories minimise the error covariance of the underlying tracker (Fig. 12). On the other hand, the sensor trajectories scheduled by maximising ExpReward (or TrFIM) show no cooperative movement between the sensors while they are approaching the target and generate large error covariance (Fig. 13).

The statistical results averaged over 100 Monte Carlo runs for each case are shown in Fig. 14, where the root-mean-squared position error comparison of the tracker under different reward functions for $N = 2$ is presented in Fig. 14 (a) and the RMS errors under DetFIM for $N = 1, 2, 3$ are in Fig. 14 (b). In summary, the simulation results demonstrate that

- the tracker gets smaller error but significant more computational overhead as N increases. We observed that the computational complexity for $N = 1, 2, 3$ is roughly at a ratio of $1 : 46 : 3304$.
- the sensor scheduling under DetFIM yield a significantly small error, which is consistent with our analysis.
- the RMS error under ExpReward is quite similar to that under TrFIM. The latter has completely ignores the correlation between the two sensor states.

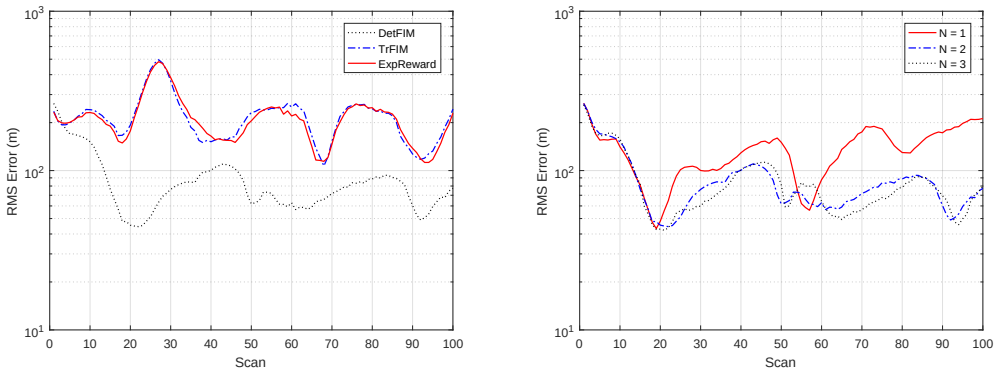

(a) (b)

Figure 14: (a) RMS errors of the estimated target trajectory with sensor trajectories optimised under different reward methods for a $N = 2$-step ahead decision process. (b) RMS errors of the estimated target trajectory with sensor trajectories optimised under DetFIM for N = 1,2,3.

2.3.3 Summary

Sensor trajectory optimisation plays an important role for tracking a moving target using multiple cooperative passive sensors. The problem is formulated as POMDP and a N-step ahead sensor trajectory scheduling is considered to steer the measurement decision process that maximises a reward function. Two statistical reward functions, the Expected Rényi Divergence and determinant of Fisher information matrix, both of which are derived in closed-forms, are considered. We show that the Expected Rényi Divergence function approximated through linearization has a significantly weak correlation between the two sensor states and thus the trajectory scheduling performance using it is as poor as using the Trace of FIM. On the other hand, the Determinant of FIM is an appropriate statistical reward function to be used. This conclusion is confirmed by the simulation results presented. Although this work is based on tracking a moving target by two bearing-only sensors scenario, the results can also be applied to other types of sensors which are required to be used jointly to observe the underlying target state, such as Doppler radars.

3 List of Publications and Significant Collaborations

In standard format showing authors, title, journal, issue, pages, and date, for each category list the following: a) papers published in peer-reviewed journals, b) papers published in peer-reviewed conference proceedings, c) papers published in non-peer-reviewed journals and conference proceedings, d) conference presentations without papers, e) manuscripts submitted but not yet published, and f) provide a list any interactions with industry or with Air Force Research Laboratory scientists or significant collaborations that resulted from this work.

1. Published papers (Journal name, title, date):

   [1] Keith Ing, Mark R. Morelande, Sofia Suvorova, and Bill Moran. Parametric texture estimation and prediction using measured sea clutter data. *IET Radar, Sonar & Navigation*, pages 1–10, 2015.

   [2] Z. Zhang, E.K.P. Chong, A. Pezeshki, and W. Moran. String submodular functions with curvature constraints. *Automatic Control, IEEE Transactions on*, 61(3):601–616, March 2016.

   [3] Pakorn Poksawa, Liuping Wang, and Abdulghani Mohamed. Automatic tuning of attitude control system for fixed-wing unmanned aerial vehicles. *IET Control Theory & Applications*, July 2016.

   [4] Jiahua Zhu, Xuezhi Wang, Xiaotao Huang, Sofia Suvorova, and Bill Moran. Range sidelobe suppression for using golay complementary waveforms in multiple moving target detection. *Signal Processing*, 141:28 31, 2017

   [5] Jiahua Zhu, Xuezhi Wang, Xiaotao Huang, Sofia Suvorova, and Bill Moran. Detection of moving targets in sea clutter using complementary waveforms. *Signal Processing*, 146:15 21, 2018.

   [6] Jiahua Zhu, Xuezhi Wang, Xiaotao Huang, Sofia Suvorova, and Bill Moran. Golay Complementary Waveforms in Reed-Muller Sequences for Radar Detection of Nonzero Doppler Targets. *Sensors*, 18(1), 2018.

   [7] Jiahua Zhu, Xuezhi Wang, Yongping Song, Xiaotao Huang, and Bill Moran. Range sidelobe suppression using complementary sets in distributed multistatic radar networks. *Sensors*, 18(1), 2018.

2. Paper currently under review (journal name, title, date accepted):

[1] W. Dang, A. Pezeshki, S.D. Howard, B. Moran, and R. Calderbank. Complementary waveforms and Doppler-induced sidelobes. IEEE Transactions on Information Theory, 2016 (in preparation).

[2] J. Zhu, X. Wang, X. Huang and B. Moran. Alternative Signal Processing of Complementary Waveform Returns for Range Sidelobe Suppression. 2018 (in preparation).

[3] X. Wang, B. Ristic, B. Himed and B. Moran. Cooperative Sensing with Passive Mobile Sensors for Target Tracking. 2018. Under review (submiited to Journal of Information Fusion).

[4] Y. Yang, B. Moran, X. Wang, T. Brown, S. Williams and Q. Pan. Experimental Analysis of Game Theoretic Formulation of Target Tracking. 2018. Under review (submitted to IEEE trans. signal processing).

3. Conference paper/poster/presentation (conf. name, title, date):

[1] Y. Yang, T. Brown, B. Moran, X. Wang, Q. Pan, and Y. Qin. A comparison of iteratively reweighted least squares and kalman filter with em in measurement error covariance estimation. In *Fusion 2016*, Heidelberg, Germany, 5-8 July 2016.

[2] J. Zhu, X. Wang, X. Huang, S. Suvorova, and B. Moran. Detection of nonzero doppler targets using complementary waveforms in reed-muller sequences. In *The 8th International Conference on Signal Processing Systems (ICSPS 2016)*, Auckland, New Zealand, 21-24, November 2016.

[3] X. Wang, B. Ristic, B. Himed, and B. Moran. Joint passive sensor scheduling for target tracking. In *2017 20th International Conference on Information Fusion (Fusion)*, pages 17, July 2017

4. Invited talks (event name, title, date):

(a) Australian Mathematical Sciences Institute (AMSI) January 2016 presentation: "Pas de Deux Mathematics and Engineering" – Prof Bill Moran

(b) DSTG workshops, Adelaide:

- 26 April 2016, "AOARD Project 2016 Presentation" – Prof Bill Moran
- 16 June 2016, "Golay-Rudin-Shapiro" – Prof Bill Moran

(c) Joint Seminar (University of Melbourne, RMIT University and DSTG Melbourne):

(d) 10 March 2016, AFRL Lab Dayton, "AOARD Project Presentation"–Prof Bill Moran

Note: AOARD Project 2015-2016 Presentation slides submitted to AOARD on July 2016.

5. Visited AFRL/DoD installation with AOARD WoS program (Location, date):

- 10 March 2016 — Prof Bill Moran has visited Dr Braham Himed, AFRL, Dayton.
- 16 April 2016 — Dr Braham Himed visited Prof Bill Moran at RMIT University, Melbourne.
- 20 July 2016 — Prof Bill Moran has visited Dr Braham Himed, AFRL, Dayton.
- 24 March 2017 — Dr Braham Himed visited Prof Bill Moran *et. al.* at RMIT University, Melbourne.
- 16 August 2017 — Prof Bill Moran has visited Dr Braham Himed, AFRL, Dayton.

4 Conclusions

In this report, we summarise the research work carried out during 2016-2017 under the AOARD project with grant no. FA2386-15-1-4066. The major work includes

1. **Radar waveform scheduling** — address the sidelobe issues induced by Golay complementary waveforms in the presence of multiple nonzero Doppler targets;
2. **Game theoretical formulation for target tracking** — study the behaviour of autonomous steering and tracking scenario involving two moving platforms chasing each other with similar sensing and kinematic motion capacities.
3. **Sensor trajectory optimisation** — continue investigating the optimality of the expected reward functions for sensor trajectory optimisation under the scenario of tracking a moving target using two cooperative bearings-only moving sensors. Explanation of the practical reward functions in the action of steering sensors from the information geometry viewpoint is presented.

Whenever possible, we will seek funding support opportunity to continue working in these research directions, in particular, in the area of autonomous mobile sensor network management and trajectory optimisation, cognitive sensing and target tracking in the game theoretic formulation environment.

References

[1] Bill Moran *et. al.* Aoard/afrl annual technical report i: "radar control – optimal resource allocation – uav tracking" (2015-2016). Technical report, Signal Processing and Sensor Control Group, School of Engineering, RMIT University, May 2016. Grant No. FA2386-15-1-4066.

[2] Bill Moran *et. al.* Aoard/afrl annual technical report ii: "radar control – optimal resource allocation – waveform scheduling, game theoretic formation of uav tracking" (2016). Technical report, Signal Processing and Sensor Control Group, School of Engineering, RMIT University, November 2016. Grant No. FA2386-15-1-4066.

[3] R. Calderbank, S. D. Howard, and B. Moran. Waveform diversity in radar signal processing. *IEEE Signal Processing Magazine*, 26(1):32–41, Jan 2009.

[4] A. Pezeshki, A. R. Calderbank, W. Moran, and S. D. Howard. Doppler resilient Golay complementary waveforms. *IEEE Transactions on Information Theory*, 54(9):4254–4266, Sep 2008.

[5] W. Dang, A. Pezeshki, S. Howard, W. Moran, and R. Calderbank. Coordinating complementary waveforms for sidelobe suppression. In *2011 Conference Record of the Forty Fifth Asilomar Conference on Signals, Systems and Computers (ASILOMAR)*, pages 2096–2100, Nov 2011.

[6] W. Dang, A. Pezeshki, S. Howard, and W. Moran. Coordinating complementary waveforms across time and frequency. In *2012 IEEE Statistical Signal Processing Workshop (SSP)*, pages 868–871, Aug 2012.

[7] S. Suvorova, S. Howard, and B. Moran. Application of Reed-Muller coded complementary waveforms to target tracking. In *2013 International Conference on Radar*, pages 152–156, Sep 2013.

[8] Y. Yang, T. Brown, B. Moran, X. Wang, Q. Pan, and Y. Qin. A comparison of iteratively reweighted least squares and kalman filter with em in measurement error covariance estimation. In *Fusion 2016*, Heidelberg, Germany, 5-8 July 2016.

[9] Jiahua Zhu, Xuezhi Wang, Xiaotao Huang, Sofia Suvorova, and Bill Moran. Golay complementary waveforms in reedmller sequences for radar detection of nonzero doppler targets. *Sensors*, 18(1), 2018.

[10] Jiahua Zhu, Xuezhi Wang, Xiaotao Huang, Sofia Suvorova, and Bill Moran. Detection of moving targets in sea clutter using complementary waveforms. *Signal Processing*, 146:15 – 21, 2018.

[11] Jiahua Zhu, Xuezhi Wang, Yongping Song, Xiaotao Huang, and Bill Moran. Range sidelobe suppression using complementary sets in distributed multistatic radar networks. *Sensors*, 18(1), 2018.

[12] M. Golay. Complementary series. *IRE Trans. Inform. Theory*, 7(2):82–87, 1961.

[13] M. A. Richards. *Fundamentals of Radar Signal Processing.* NY: McGraw-Hill Education, 2005.

[14] S. Suvorova, S. Howard, B. Moran, R. Calderbank, and A. Pezeshki. Doppler resilience, Reed-Muller codes and complementary waveforms. In *2007 Conference Record of the Forty-First Asilomar Conference on Signals, Systems and Computers*, pages 1839–1843, Nov 2007.

[15] W. Dang. Signal design for active sensing. *Ph. D Dissertation, Colorado State University*, 2014.

[16] J. Zhu, X. Wang, X. Huang, S. Suvorova, and B. Moran. Detection of nonzero doppler targets using complementary waveforms in reed-muller sequences. In *The 8th International Conference on Signal Processing Systems (ICSPS 2016)*, Auckland, New Zealand, 21-24, November 2016.

[17] S. M. Kay. *Fundamentals of Statistical Signal Processing, Vol II - Detection Theory.* Prentice Hall, 1998.

[18] Jiahua Zhu, Xuezhi Wang, Xiaotao Huang, Sofia Suvorova, and Bill Moran. Range sidelobe suppression for using golay complementary waveforms in multiple moving target detection. *Signal Processing*, 141:28 – 31, 2017.

[19] U. K. Majumder, M. R. Bell and M. Rangaswamy, "A novel approach for designing diversity radar waveforms that are orthogonal on both transmit and receive," *IEEE Radar Conf.*, 2013, pp. 1-6.

[20] W. Q. Wang, "Space-time coding MIMO-OFDM SAR for high-resolution imaging," *IEEE Trans. Geosci. Remote Sens.*, 2011, **49**(8), pp. 3094-3104.

[21] S. Searle, S. Howard and B. Moran, "The use of complementary sets in MIMO radar," *42nd Asilomar Conf. Signals, Systems and Computers*, 2008, pp. 510-514.

[22] S. Searle and S. Howard, "Waveform design and processing for multichannel MIMO radar," *Int. Radar Conf.*, 2009, pp. 1-6.

[23] J. Zhu, X. Wang, X. Huang, *et al.*, "Range sidelobe suppression for using Golay complementary waveforms in multiple moving target detection," *Signal Process.*, 2017, **141**, pp. 28-31.

[24] M. Golay, "Complementary series," *IRE Trans. Inform. Theory*, 1961, **7**(2), pp. 82-87.

[25] C. C. Tseng and C. Liu, "Complementary sets of sequences," *IEEE Trans. Inform. Theory*, 1972, **18**(5), pp. 644-652.

[26] http://www.tek.com/datasheet/arbitrary-waveform-generators-1.

[27] X. Wang, B. Ristic, B. Himed, and B. Moran. Joint passive sensor scheduling for target tracking. In *2017 20th International Conference on Information Fusion (Fusion)*, pages 1–7, July 2017.

[28] N. H. Abdel-All, H. N. Abd-Ellah, H. M. Moustafa, Information geometry and statistical manifold, Chaos, Solitons and Fractals 15 (1) (2003) 161–172.

[29] P. Petersen, Riemannian geometry, Springer, New York, 1998.

[30] X. Wang, M. Morelande and B. Moran. "Target Motion Analysis Using Single Sensor Bearings-Only Measurements", *Proceedings of the 2nd International Conference on Image Processing and Signal Processing (CISP'09)*, pp. 2094–2099, Tianjin, China, 17 - 19, Oct. 2009.

[31] D. Musicki. Multi-target tracking using multiple passive bearings-only asynchronous sensors. *IEEE Transactions on Aerospace and Electronic Systems*, 44(3):1151–1160, July 2008.

[32] Z. Yang, J. Laaksonen, Principal whitened gradient for information geometry, Neural Networks 21 (2-3) (2008) 232–240.

[33] Zach Fuchs, Bill Moran and Simon Williams. "Trajectory planning with Radar", white paper, August, 2017.